Research Square

Preprints are preliminary reports that have not undergone peer review.
They should not be considered conclusive, used to inform clinical practice,
or referenced by the media as validated information.

# Local proximal tubule complement contributes to maladaptive repair in rhabdomyolysis-induced acute kidney injury and escapes systemic inhibition

**Anne Grunenwald**
Centre de Recherche des Cordeliers
**Idris Boudhabhay**
Centre de Recherche des Cordeliers
**Margot Revel**
Centre de Recherche des Cordeliers
**Victoria Poillerat**
Centre de Recherche des Cordeliers
**Mikel Rezola Artero**
Centre de Recherche des Cordeliers
**Sara Soares Tozoni**
Centre de Recherche des Cordeliers
**Alaeddine Redissi**
Centre de Recherche des Cordeliers
**Elodie Voilin**
Centre de Recherche des Cordeliers
**Emma Fleury**
Centre de Recherche des Cordeliers
**Julie Peliconi**
Centre de Recherche des Cordeliers
**Alessandra Zarantonello**
Centre de Recherche des Cordeliers
**Gilles Crambert**
Centre de Recherche des Cordeliers
**Andrea Novais Moreno Amaral**
Pontifícia Universidade Católica do Paraná, Curitiba, Brazil
**Steven Sacks**
King’s College London
**Viviane Gnemmi**
CHU Lille
**Marie Frimat**

CHU Lille

**Jean-Paul Duong-Van-Huyen**

Centre de Recherche des Cordeliers

**Nicolas S Merle**

Centre de Recherche des Cordeliers

**Lubka Roumenina**

lubka.roumenina@sorbonne-universite.fr

Centre de Recherche des Cordeliers

---

**Research Article**

**Keywords:** acute kidney injury, complement system, maladaptive repair, proximal tubule, rhabdomyolysis

**Posted Date:** June 11th, 2026

**DOI:** https://doi.org/10.21203/rs.3.rs-9932397/v1

**License:** This work is licensed under a Creative Commons Attribution 4.0 International License.
Read Full License

**Additional Declarations:** The authors declare potential competing interests as follows:

---

# Abstract

**Background and hypothesis**: Maladaptive repair drives progression from acute kidney injury (AKI) to chronic kidney disease. Injured proximal tubular cells overexpress complement C3 mRNA, but its functional role is not well understood. We hypothesized that complement proteins produced and active locally within proximal tubules drive maladaptive repair and remain inaccessible to plasma-targeted inhibitors.

**Methods**: We investigated complement, encompassing extracellular, autocrine and intracellular pools, in human biopsies and mouse model of rhabdomyolysis-induced AKI (RIAKI). Hyperplex sequential immunofluorescence combined with RNAscope was used to localize complement proteins and transcripts *in situ* and immune infiltrate. C3 or factor B (FB) deficient mice and pharmacological FB inhibition were tested in a RIAKI model. Bulk transcriptomics and C3/CFB knockdown in tubular cells with rescue experiments dissected mechanisms *in vivo* and *in vitro*.

**Results**: In human and experimental RIAKI, injured VCAM-1 proximal tubules showed reabsorption and local transcription of C3 and CFB in a subset of tubules, induced by inflammatory cytokines. Genetic deletion of *C3* or *Cfb* attenuated AKI, reducing tubular necrosis, immune infiltration and signatures of epithelial-to-mesenchymal transition and maladaptive repair. Pharmacological FB inhibition reduced extracellular C3 activation but did not preserve renal function. *In vitro*, C3 or FB knockdown in tubular cells suppressed proliferation, inflammation and mTOR-linked metabolic pathways and was not rescued by exogenous purified protein, consistent with cell-intrinsic/intracellular mode of action.

**Conclusion**: Locally produced complement in proximal tubules drives inflammatory and maladaptive repair programs during AKI. The dissociation between genetic deletion and pharmacological FB inhibition indicates that the relevant complement activity occurs in a compartment poorly accessible to systemic inhibitors and supports development of locally acting, tissue-penetrant or cell-permeable complement-targeted therapies for AKI.


# Key learning points

**What was known:** Complement activation accompanies AKI and complement-deficient mice are protected, yet systemic complement inhibitors have shown limited benefit in AKI and ischemia-reperfusion trials. Injured proximal tubular cells can locally synthesise complement components C3 and factor B.

**This study adds:** Local and intracellular proximal tubule complement drives inflammatory and maladaptive repair programs in rhabdomyolysis-induced AKI. Genetic deletion of *C3* or *Cfb* is protective, whereas systemic FB inhibition reduces extracellular C3 deposition without preserving renal function.

**Potential impact:** The failure of plasma-targeted complement inhibitors in AKI may reflect inadequate access to the relevant tubular compartment rather than evidence against complement as a target.

Locally acting, tissue-penetrant or cell-permeable complement inhibitors are a rational next step.

# Introduction

Proximal tubular cells (PT) are both targets and drivers of inflammation, and their injury underlies acute kidney injury (AKI) and maladaptive repair(1–3). Maladaptive repair, marked by persistent VCAM-1 expression (4), sustained inflammation, epithelial-to-mesenchymal transition (EMT), and fibrosis, drives long-term renal outcome and the AKI-to-CKD transition.

Complement system is implicated in AKI, yet systemic inhibitors have not translated into clinical benefit(5). Although most plasma complement is liver-derived, many cell types synthesize components locally, including C3 and factor B (FB)(6). Upon activation, PT express C3 and secrete cytokines that recruit macrophages and amplify damage(2, 6–9). Whether PT-intrinsic C3 is a bystander or a functional driver of maladaptive repair remains unclear. In other cell types, intracellular complement regulates metabolism and inflammatory signaling beyond the extracellular cascade(10–16).

We hypothesized that C3 and FB produced and acting locally within PT, rather than within the circulating cascade, contribute to maladaptive repair. We used rhabdomyolysis-induced AKI (RIAKI), a clinically relevant model of sterile epithelial stress(17), in which strong intracellular C3 staining in injured PT and protection in C3-deficient mice support a complement role in tubular injury(9, 18, 19).

To test this, we leveraged our in situ complementomics platform(20) for spatial complement mapping on human RIAKI biopsies, combined with genetic and pharmacological complement manipulation in mice and loss-of-function studies in PT cells. We show that locally produced C3 and FB in PT reprogram inflammatory, metabolic, proliferative, and detoxification pathways and amplify maladaptive repair. The compartmentalisation of this activity, beyond the reach of plasma-targeted inhibitors, may explain the limited efficacy of systemic complement therapeutics in AKI and supports a rationale for tissue-penetrant or cell-permeable inhibitors.

# Materials and Methods

Detailed methods are provided in the Supplementary Material.

**Human samples and spatial analysis.**

FFPE kidney biopsies from seven patients with RIAKI (Supplementary Table 1) and three peri-tumoral controls from clear cell renal cell carcinoma (ccRCC) were analysed by sequential immunofluorescence (seqIF™, COMET™ platform, Bio-Techne Spatial) using a validated 14-marker in situ Complementomics panel(20). SeqIF was also combined with RNAscope™ HiPlex Pro for *C3* and *CFB* mRNA co-detection. Single-nuclei RNA-seq data from normal (tumor-adjacent) kidney tissue were re-analyzed in R/Seurat with GSEA against MSigDB Hallmark gene sets. All patients gave written informed consent and the research was performed in accordance with the Declaration of Helsinki.

**Animal models.**

Male C57BL/6 wild-type, *C3*$^{-/-}$ and *Cfb*$^{-/-}$ mice received 200 µL 50% glycerol intramuscularly under isoflurane anaesthesia and were sacrificed at 24 h. In selected experiments the oral FB inhibitor CPX014 (1.2 mg/mouse) was given 90 min before and 10.5 h after glycerol. Muscle injury was assessed by ASAT to ensure similar level of muscle injury across conditions. Kidney function, histology, complement deposition and apoptosis (TUNEL) were analysed using HALO software. Immune infiltrate was inferred from bulk RNA-seq using mMCP-counter tool (21). Experiments were approved by the Charles Darwin ethical committee (APAFIS#2148).

**In vitro studies.**

RPTEC, HK-2 and Caki-1 cells were stimulated with TNFα, IL-1β or IL-6 (10 ng/mL) and gene expression measured by QuantiGene. Caki-1 was selected for FB studies because of the higher detectable basal FB. Key C3 findings were confirmed in HK-2. Cells were transfected with siRNAs against *C3 or CFB* (RNAiMAX, 50 nM, 72 h). Proliferation (CFSE) and mortality (DAPI) were assessed by flow cytometry. Rescue used purified C3 or FB. Complement proteins and fragments were measured by ELISA and Western blot. Targeted metabolomics used cold-methanol extraction with MetaboAnalyst pathway analysis. Bulk RNA-seq was performed on Illumina with DESeq2, GSEA and SignalR ligand–receptor analysis. Full methods are provided in the Supplementary Material.

# Statistical analysis.

Statistical analyses were performed using GraphPad Prism and R. Non-parametric tests were applied as appropriate, with $p < 0.05$ considered statistically significant.

## Results

# C3 and FB presence reflect both reabsorption and local synthesis in VCAM-1 positive injured PT

We developed a sequential immunofluorescence (seqIF) antibody panel to detect complement proteins, immune cells, and tubular markers (*in situ* Complementomics)(20). *In situ* Complementomics analysis of 7 RIAKI biopsies (Supplementary Table 1), compared with normal controls, revealed intracellular granular C3 and FB staining in PT (defined as megalin-positive), (Fig. 1A–C). PT have a high reabsorptive capacity, making it difficult to distinguish locally synthesized proteins (mRNA–protein colocalization) from reabsorbed proteins (protein without mRNA). To address this, we combined seqIF with RNAscope for C3 and FB. This approach identified tubules displaying protein-only staining, suggesting reabsorption (Figure S1), as well as tubules positive for both mRNA and protein, supporting local synthesis of C3 and FB (Fig. 1B,D). C3 and FB staining partially co-localized in ~ 35% of tubules (Fig. 1D). All staining patterns

were observed within the same biopsies (Fig. 1D). PT expressing *C3* and/or *FB* mRNA were most frequently VCAM1-positive, consistent with an activated/injured tubular state (Fig. 1E).

## Complement-expressing PT carry an inflammatory and stress-response signature

We extracted the signature of $C3^+$ or $CFB^+$ human PT from a snRNAseq dataset (peritumoral kidney(22)) (Fig. 2A,B). In this state, only 2.4% of PT expressed C3 and 5.6% expressed *CFB*, in line with the scarce protein staining in controls (Fig. 1C). Notably, $C3^+$ and $CFB^+$ PT showed enrichment of inflammatory hallmark pathways, including IFN-γ, IL-6, and TNF-α responses (Fig. 2A,B), suggesting an association of *C3* and *CFB* expression with immune-mediated PT stimulation.

## Complement-expressing tubules localize within a complement-responsive myeloid infiltrate

*In situ* Complementomics enabled mapping of the immune microenvironment in RIAKI kidney biopsies (Fig. 2C–J). RIAKI kidneys showed increased infiltration of T and B cells (Fig. 2C–E), forming lymphoid aggregates in 4 of 7 patients, as well as elevated macrophage ($CD68^+$) and neutrophil ($CD68^-CD11b^+$) infiltration (Fig. 2C,F,G). Although the proportion of $CD68^+$ macrophages expressing CD163 was similar to controls (Fig. 2H,I), $CD68^+CD163^+$ macrophages expressing C5aR1 were markedly increased in RIAKI kidneys (median 63% vs 4% in controls; Fig. 2J). These macrophages localized near $C3^+$ tubules (Fig. 2C), consistent with our prior observations(9, 18) and suggesting a complement-driven pro-inflammatory phenotype.

# Inflammatory cytokines from the immune infiltrate induce tubular C3 and FB expression

We confirmed that PT express *C3* and *CFB* mRNA under inflammatory conditions *in vitro* in two cell lines (HK2 and Caki-1) and in primary cells (RPTEC) using QuantiGene (Fig. 2K,L; Figure S2A,B). C3 protein was detectable in HK2 cells (Figure S2C), whereas FB protein was low; therefore, the higher FB-expressing Caki-1 line was used for FB analyses (Figure S2D). Even if of tumor origin, Caki-1 cells do not carry VHL mutation and are suitable model to explore PT(23) Efficient knockdown of C3 or FB was confirmed by loss of the corresponding bands in supernatants of siC3 and siFB cells compared with controls (Figure S2C,D). C3 and FB expression was increased by AKI-relevant cytokines IL-1β or TNF-α, but not IL-6, across all PT models tested (Fig. 2K,L; Figure S2E,F). These findings prompted further investigation of the coordinated and distinct roles of C3 and FB in PT during inflammatory stress.

**Genetic loss of C3 or Cfb attenuates tubular injury after glycerol-induced rhabdomyolysis**

We analyzed *Cfb*$^{-/-}$ and *C3*$^{-/-}$ mice compared to WT in a glycerol-induced RIAKI model (Fig. 3). Both genotypes showed preserved kidney function, with urea levels remaining within the normal range despite muscle injury assessed by ASAT elevation (Fig. 3A; Figure S3). Consistently, *Cfb*$^{-/-}$ and *C3*$^{-/-}$ mice exhibited fewer myoglobin casts, reduced acute tubular necrosis, decreased C3 staining, and less cell death compared with WT mice (Fig. 3B–D), as previously reported for *C3* deficiency(18).

**RIAKI triggers a consistent maladaptive repair response in which complement appears to play a role.**

To understand why congenital *C3* or *Cfb* deficiency protects against RIAKI, we performed bulk RNAseq. As the transcriptomic analyses derived from three independent *in vivo* experiments, we first assessed the reproducibility of the RIAKI model by comparing our previously published dataset(18) with two newly generated datasets (FB inhibition and *Cfb*$^{-/-}$ experiments, see below). All three showed highly comparable enrichment of Hallmark gene sets in WT glycerol-treated mice compared with PBS controls (Figure S4A), including inflammation, epithelial-to-mesenchymal transition (EMT), tissue injury, and complement pathways. Complement-related ligand–receptor interactions were significantly increased (Figure S4B). Broader ligand–receptor analyses further revealed pathways associated with maladaptive repair and fibrosis, including CD44 signaling, integrin–collagen interactions, Rho GTPase–mediated cell adhesion and cell-cycle regulation, and extracellular matrix (ECM) organization involving VCAM1 (Figure S4C), consistent with fibrotic progression at later disease stages(9, 24). Of note, *C3* and *Cfb* were also upregulated in PT in mouse models of ischemia/reperfusion injury (25), suggesting a broader relevance of this process.

**C3 or Cfb deficiency disengages the maladaptive repair program**

Comparative transcriptomic analysis of *Cfb*$^{-/-}$ and *C3*$^{-/-}$ mice, at baseline and after glycerol-induced RIAKI, revealed protective programs relative to WT (Fig. 4A–E). At baseline, C3$^{-/-}$ kidneys (versus WT) displayed 388 down- and 372 upregulated genes (Fig. 4A), with negative enrichment of inflammatory (TNF-α/IFN-γ/IL-6/IL-2, complement), apoptotic, EMT, and mTOR pathways, accompanied by reduced T cell and fibroblast signatures (Fig. 4A,D), indicating a lowered basal inflammatory tone. Following injury, both *Cfb*$^{-/-}$ and *C3*$^{-/-}$ glycerol-treated kidneys showed attenuated transcriptomic perturbation compared with WT despite muscle damage (Figure S3), with 1,421/973 and 1,440/872 up- and down-regulated DEG, respectively (Fig. 4B,C upper panels; Figure S5). In both models, ligand–receptor interactions were less altered (Figure S6), and GSEA revealed preserved metabolic programs, including oxidative phosphorylation (OXPHOS), fatty acid, bile acid, and xenobiotic metabolism (Fig. 4B,C, bottom panels), alongside suppression of inflammatory signaling, EMT, mTOR, cell–cell interaction, and cell-cycle/proliferative pathways. These transcriptional features correlated with reduced infiltration of inflammatory monocytes in glycerol-treated *Cfb*$^{-/-}$ and *C3*$^{-/-}$ kidneys (Fig. 4D). Comparative DEG analysis confirmed convergence between the two models, with ~ 22% overlap after injury (Fig. 4E; Supplementary Data file 1), defining a shared protective signature characterized by enhanced heme detoxification and mitochondrial metabolism, preserved PT identity, and broad repression of inflammatory, fibrotic, and stress-response pathways, including key mediators of leukocyte recruitment

and ECM remodeling. Together, these data indicate that C3 and FB deficiency confer transcriptional programs that limit inflammation, maladaptive repair, and proliferative stress, thereby reducing kidney susceptibility to AKI.

**Systemic FB inhibition reduces complement activation but does not protect against tubular injury or maladaptive repair**

Given the protection from RIAKI observed in *Cfb*$^{-/-}$ and *C3*$^{-/-}$ mice, we tested whether this phenotype depended on activation of the plasma complement cascade by inhibiting FB with CPX014 (a surrogate for LNP023/iptacopan)(26). Pharmacological FB inhibition targets the enzymatic activity of circulating and extracellular FB but does not eliminate the cell-intrinsic/intracellular FB pools; therefore, genetic and pharmacological approaches are not necessarily equivalent. FB inhibition failed to prevent AKI, as assessed by plasma urea levels and renal cell death (Fig. 5A,B; Figure S7), and to prevent the C3 overexpression (6-fold in the glycerol-treated mice, compared to WT), despite effective suppression of tubular C3b/iC3b staining (Fig. 5C,D). CPX014 had no effect on gene expression in PBS-treated mice (Fig. 5E), and transcriptomic comparison of glycerol-injected WT kidneys with or without CPX014 revealed only minor changes (Fig. 5F). Inflammatory monocyte infiltration was similarly unaffected (Fig. 5G), and ligand–receptor interaction patterns attenuated in *Cfb*$^{-/-}$ mice were not reproduced by FB inhibition (Figure S8).

Together, these data indicate that C3 and FB promote kidney injury in RIAKI through mechanisms independent of the plasma complement cascade, supporting a role for cell-intrinsic, tubular-derived complement functions. As PT dominate the renal transcriptomic signal(27) and are major sources of C3 and FB in patient biopsies, we next examined cell-intrinsic complement functions in tubular models *in vitro*. This *in vitro* validation in PT cells was a necessary step, as the mice had global *C3* or *Cfb* deficiency, and other C3 and FB expressing cells could contribute to the kidney protective phenotype.

**Loss of FB in PT cells reproduces the anti-inflammatory, anti-proliferative and metabolic reprogramming observed in vivo**

FB knockdown in Caki-1 cells (Figure S2D) resulted in 745 upregulated and 951 downregulated genes (Fig. 6A). GSEA revealed positive enrichment of metabolic and DNA repair programs (Figure S9A,B), the latter likely reflecting an *in vitro*–specific stress response, as increased cell mortality was observed in culture (Figure S9C), whereas *Cfb*$^{-/-}$ mice showed preserved renal histology and no excess cell death even after glycerol injury (Fig. 3B,D). Consistent with the *in vivo* phenotype, inflammatory (TNFα/IFNγ/IL-2/IL-6) and cell-cycle–related gene sets were negatively enriched, indicating suppression of inflammatory and proliferative responses (Figure S9A,B).

Comparison of differentially expressed genes (DEGs) shared between *Cfb*$^{-/-}$ glycerol-treated kidneys vs glycerol-treated WT; and siFB cells vs siC identified 53 commonly upregulated and 64 downregulated transcripts (Fig. 6B), with concordant enrichment of xenobiotic metabolism, OXPHOS, and adipogenesis (Fig. 6C). Shared upregulated genes included PT transporters and metabolic enzymes associated with

preserved epithelial differentiation and solute handling (Supplementary Data file 1), consistent with the protective phenotype observed *in vivo* (Figs. 2,3).

Integrated pathway and DEG analyses confirmed that FB deficiency *in vitro* and *in vivo* suppresses inflammatory and immune transcriptional programs, including cytokine and chemokine signaling, interferon-stimulated pathways, and NF-κB and AP-1 effectors, as well as fibrotic and ECM remodeling programs (Fig. 6C; Supplementary Data file 1). Suppression of cell-cycle and mitotic regulators paralleled reduced proliferation measured *in vitro* (Fig. 6D). Importantly, neither reduced proliferation nor viability could be rescued by the addition of extracellular purified FB (Fig. 6D; Figure S9C), consistent with intracellular action and insufficient capacity of the cell to uptake and use the supplemented protein.

Despite transcriptional enrichment of OXPHOS, metabolomic profiling revealed broad reductions in intracellular metabolites, including amino acids, with pathway analysis indicating downregulation of amino acid metabolism (Fig. 6E,F). This was associated with reduced expression of biosynthetic enzymes and amino acid transporters, including LAT1 (Supplementary Data file 1), suggesting that enhanced OXPHOS signatures reflect compensatory transcriptional adaptation to an underlying metabolic deficit.

## Loss of C3 in PT cells reproduces key features of the protective in vivo phenotype

C3 knockdown resulted in 92 up- and 97 downregulated genes in HK2 cells and 437 up- and 549 downregulated genes in Caki-1 cells (Figures S2C; 7A,B; S10A,B; S11A,B), without affecting cell viability, morphology, or 3D interaction capacity (Figure S11C–E).

In agreement with *in vivo* findings, siC3 cells showed enrichment of xenobiotic metabolism and metabolic reprogramming pathways, with negative enrichment of cell-cycle/proliferation and mTOR gene sets in both models (Fig. 7C,D). Reduced proliferation was confirmed functionally (Fig. 7E,F; Figure S11G,H) and was not rescued by extracellularly added purified C3, consistent with an intracellular requirement that cannot be replenished by exogenous protein. The similarity of the phenotype of HK2 and Caki-1 cells and the mouse model supports biological convergence despite the transformed background of Caki-1 and validate its use here as a PT model(23). At the whole-organ level, inflammatory pathways were reduced in $C3^{-/-}$ kidneys, consistent with MCP-counter analysis showing diminished immune-cell infiltration, while inflammatory hallmark pathways were enriched in siC3 cells.

Across all C3-deficient conditions, common upregulated genes included AQP3 and FLVCR2, the latter conferring protection against heme overload(28), in line with an upregulation of the heme-degrading enzyme *HMOX1* in both siC3 models at mRNA and protein levels (Figure S10A,B; Figure S11F). Importantly, this profile was not recapitulated in siFB cells, suggesting a C3-specific, FB-independent cytoprotective response to heme stress.

## Cell-intrinsic C3 regulates PT phenotype

In C3-deficient glycerol-treated mice vs glycerol-treated WT; and siC3 cells vs siC, mTORC1-linked metabolic pathways were consistently negatively enriched (Fig. 7D), accompanied by coordinated downregulation of mTOR-associated genes (Supplementary Data file 1). Metabolic profiling of siC3 Caki-1 cells revealed altered glycolysis, with increased intracellular glucose despite unchanged GLUT1 expression, while most other metabolites were unchanged or reduced, indicating broad metabolic reprogramming (Fig. 7G,H).

Cell metabolism and mTOR signaling have been linked to intracellular C3 cleavage into C3a-like fragment signaling in lysosomes (13). Consistently, C3 was detected in organelle-enriched fractions of Caki-1 and HK2 cells, and partially colocalizing with lysosomes (Fig. 7I; Figure S12A–C), together with detectable C3aR expression (Figure S11I, S12D). Moreover, siC3 results in decreased ribosomal protein S6 phosphorylation, without significant change in AKT phosphorylation, supporting the decreased mTORC1 activity, deduced by the RNAseq (Figure S11J,K). C3 was also present in the nucleus in processed (α/β chains) and unprocessed forms, as well as unprocessed in the cytosol (Fig. 7I; Figure S12A,B), similar to previous observations in pancreatic β-cells(12). Intracellular C3a was detected in Caki-1 lysates (Fig. 7J).

C3a may be generated intracellularly by a C3 convertase or by proteolytic cleavage, such as by cathepsin L(13–15). Processed C3 was detected intracellularly (Fig. 7I), while FB cleavage fragments were present but at the detection limit (Ba 0.66 ± 0.017 ng/ml; Bb 0.04 ± 0.0078 ng/ml; n = 4). Knockdown of FB or FH tended to reduce intracellular C3a-like levels (Fig. 7J), suggesting a limited contribution of a convertase, distinct from FH-regulated mechanisms described in macrophages(14, 29). Cathepsin L expression was detected in PT *in situ* and in PT cell lines (Figure S13A–C). Together, these data are consistent with an intracellular C3a–C3aR–mTORC1 axis operating in PT, similar to that described in T cells and macrophages. Definitive discrimination between truly intracellular function and autocrine signalling by locally secreted complement will require compartment-specific genetic tools such as secretion-deficient C3 or FB mutants and cell-permeable C3aR antagonists, beyond the scope of this study.

# Discussion

Our data identify a previously unrecognized cell-intrinsic complement axis in injured PT, driven by locally produced C3 and FB and acting independently of the systemic cascade (Fig. 7K). Here we show that immune cell recruitment in AKI induces tubular C3 and FB expression, and that genetic deletion of either component, but not pharmacological FB blockade, confers protection through anti-inflammatory, anti-proliferative, anti-fibrotic, and metabolic reprogramming consistent with attenuation of maladaptive repair. Partial recapitulation by in vitro silencing of C3 or CFB in PT cells, not rescued by extracellularly added purified protein, supports a locally produced, cell-intrinsic mode of action. These findings reframe complement function in AKI as a compartmentalized tubular process and offer a plausible explanation for the limited efficacy of plasma-targeted complement inhibitors in this setting.

Protection of $Cfb^{-/-}$ and $C3^{-/-}$ mice from RIAKI, together with partial protection by C3 consumption in rodents and elevated urinary complement activation fragments in patients and mice(9, 18, 19), supports complement activation as a driver of rhabdomyolysis-induced AKI. Yet inhibition of C5 or C5aR1 failed to prevent RIAKI, and complement activation occurred after tubular injury and myeloid infiltration(9). Early cascade inhibition at the level of FB with the regiment tested here also failed to protect. Similar observations exist in ischemia–reperfusion injury (IRI)(1, 30–32), where complement-deficient mice are protected(33) but inhibitors show limited benefit(34–36). In our model, FB inhibition prevented tubular C3 staining but not C3 gene expression, suggesting staining reflects mainly reabsorption. AKI persisted, indicating that mechanisms beyond plasma cascade activation contribute to injury.

Genetic deletion removes both extracellular and intracellular complement pools, whereas current inhibitors spare intracellular and locally shed pools, pointing to locally produced complement in PT as a contributor to RIAKI and likely other forms of AKI. This compartmentalized view reconciles a long-standing paradox: complement activation is consistently observed in AKI, complement deficiency is protective in animals, yet systemic inhibitors have shown limited benefit in clinical trials of AKI, IRI, and post-cardiac-surgery AKI. This is not evidence against complement as a target, but suggests that the relevant activity occurs in a compartment poorly accessible to plasma-acting inhibitors. The implication is to develop locally acting, tissue-penetrant or cell-permeable inhibitors. Some protective transcriptional signatures in *C3-/-* mice, particularly inflammatory pathways, were not reproduced in vitro, indicating that systemic or developmental adaptations also contribute.

Sterile inflammation from injured tubules is central to RIAKI(9, 24, 37). Patient biopsies revealed lymphoid and myeloid infiltration, consistent with heme-driven tubular injury recruiting immune cells in mice(9, 24). This milieu induces tubular C3 and FB expression, in line with cytokine-responsive signatures in $C3^{+}$ and $CFB^{+}$ human PT and with IL-1β- and TNF-α-induced C3/FB expression in vitro. Reduced immune infiltration in $C3^{-/-}$ mice and anti-inflammatory reprogramming in $Cfb^{-/-}$ mice indicate that tubular complement drives immune recruitment. Reduced IL-6 in *C3*-deficient kidneys and cells, similar to the intracellular C3-dependent IL-6 regulation in T cells(16), may underlie diminished basal T-cell infiltration and suggests tubular C3 maintains a defensive inflammatory baseline but amplifies injury under stress.

In situ complementomics with RNAscope localized C3 and FB expression to VCAM-1–positive injured tubules, echoing findings in IRI and interstitial nephritis(7, 38, 39). C3 and FB deficiency reduced tubular proliferation in vivo and in vitro, implicating local complement in repair dynamics. The signatures rescued by C3 or Cfb-deficiency, persistent VCAM-1, NF-κB and TGF-β signalling driving EMT and ECM remodeling, are molecular hallmarks of maladaptive repair and the principal determinant of progression to CKD(40–42). Locally produced C3/C3a and FB promote EMT across tissues(43–45), supporting a conserved complement–EMT axis. Convergence of heme detoxification programs (HMOX1, FLVCR2) in C3-deficient kidneys and cells further suggests tubular complement modulates the response to the dominant injurious stimulus in RIAKI.

Complement deficiency consistently enhanced xenobiotic metabolism and heme-protective pathways. Upregulation of FLVCR2(28) and HO-1 likely contributes to defense against heme toxicity in RIAKI and other AKI forms(46). FB deficiency similarly dampened inflammatory signaling and altered metabolic programs, consistent with prior kidney, macrophage, and lung observations(6, 14, 47), identifying FB and to some extent C3 as positive regulators of epithelial inflammatory responses. C3 and FB deficiency is thus protective in sterile inflammation, even if deleterious in infection(48, 49).

Mechanistically, our data support intracellular C3 cleavage into a C3a-like fragment(13–15), possibly via cathepsin L or minor convertase activity. C3 detection in lysosomes and mTOR-linked metabolic control align with the C3/C3a–C3aR–mTOR axis(13–15). Cytosolic and nuclear C3 suggests additional regulatory functions requiring further study.

Several limitations apply. The *Cfb*$^{-/-}$ cohort was limited owing to SARS-CoV-2 constraints. siRNA depletion eliminates both intracellular and locally secreted pools, and failure of extracellular protein to rescue may reflect insufficient uptake or a genuinely intracellular function; definitive discrimination awaits compartment-specific tools such as secretion-deficient mutants. Finally, germline deletion may entail developmental adaptations, and acute cell-specific causality was not directly tested, as PT-specific *C3* or *Cfb*-deficient mice are unavailable to us.

In conclusion, heme-driven tubular injury initiates inflammation and immune recruitment, which induces local tubular C3 and FB expression and activity thus driving maladaptive repair beyond the reach of systemic inhibitors (Fig. 7K). The same compartmentalized biology likely extends to IRI in cardiac surgery, stroke, and transplantation(17, 50), supporting the development of tissue-penetrant or cell-permeable complement-targeted therapies to preserve epithelial integrity and limit progression to CKD.

## Declarations

Patients provided informed consent for the research use of residual renal tissue samples and associated clinical data, the collection is approved with the number DC-2026-7977, CHU Lille hospital, Lille, France.

# Conflict of interest

LTR declared research funding from CSL Behring and Novartis. AG declares lecture fees from AstraZeneca. The other authors declare no conflict of interest related to this work.

# Funding

This work is supported by the ANR project CompKid ANR-24-CE14-2619-01 to LTR, by the Svar Complement excellence award to LTR, by Fondation pour la Recherche Médicale FRM team label (FRM EQU202503020008) to LTR, by the EJPRD program of the European commission via the project EJPRD2022-016 COMPRare, through the ANR funding ANR-22-RAR4-0007-03 and INCAPLBio grant

INCa_16096 to LTR and by the France 2030 program through the Idex Université Paris Cité InFibrex project (ANR-18-IDEX-0001) grant and SFNDT grant to AG. AG and IB received a PhD fellowship from FRM. MRA was supported by funds of the EU MSCA project CORVOS 860044. LTR, ANMA and SST are supported by a grant for France-Brazil collaboration from CAPES/COFECUB # Me986/23 (dossier Campus France 49518WM).

# Author contributions

AG, IB, NM, LTR: conceptualization, data curation, formal analysis, supervision, validation, methodology, writing-original draft, writing-review and editing. AG, IB, MR, NM, VP, MRA, EV, EF, SST, AZ, AR, ANMA, JP, performed research and analyses of the data. JPDVH, MF and VG provided patient samples. SS, GC: provided vital reagents, mice and assays. All authors read and approved the manuscript.

# Acknowledgements

We are grateful to the team of the CRC core facilities CHICS and CEF for the excellent technical assistance.

# Availability of data and materials

The datasets supporting the conclusions of this article are included within the article and its supplementary files. The RNAseq dataset comparing kidney transcriptomes from normal C57Bl/6 WT and *C3*$^{-/-}$ mice, treated or not with glycerol (18) supporting the findings of this study are openly available in repository GEO at accession number GSE153507. Human control peritumoral kidney snRNAseq data was taken from Hu et al (22). Processed data were downloaded from https://zenodo.org/records/8063124, file normal_snRNA.rds. The newly generated mouse kidney RNAseq datasets of the C57Bl/6 WT and *Cfb*$^{-/-}$ mice treated with glycerol or the C57Bl/6 WT mice, injected or not with FB inhibitor CPX014 are available at 10.5281/zenodo.18644294. The cell lines RNAseq datasets of the siC and siC3 HK2 cells or Caki-1 cells as well as siC and siCFB Caki-1 cells are available as follows: at 10.5281/zenodo.13891307 - HK2 siC and siC3; at 10.5281/zenodo.18644314 – Caki-1 siC and siC3 and 10.5281/zenodo.13891430 - Caki1 siC and siFB. The clinical data of the patients is available in Supplementary Table 1.

## References

1. Sheerin NS, Risley P, Abe K, Tang Z, Wong W, Lin T et al (2008) Synthesis of complement protein C3 in the kidney is an important mediator of local tissue injury. FASEB J 22(4):1065–1072
2. Portilla D, Sabapathy V, Chauss D (2025) Role of local complement activation in kidney fibrosis and repair. J Clin Invest. ;135(12)

3. Xuanyuan Q, Wu H, Sundaramoorthi H, Isnard P, Chen C, Rahmani W et al (2025) Multimodal spatial transcriptomic characterization of mouse kidney injury and repair. Nat Commun 16(1):7567
4. Kristensen AM, Bordoni L, Nielsen MB, Faivre A, Kidmose H, Sardella D et al (2025) In vivo expression of VCAM1 precedes nephron loss following kidney tubular necrosis. Sci Adv 11(43):eadz5358
5. Lamers C, Ricklin D, Lambris JD (2023) Complement-targeted therapeutics: An emerging field enabled by academic drug discovery. Am J Hematol 98(Suppl 4):S82–S9
6. Sun ZJ, Chang DY, Chen M, Zhao MH (2022) Deficiency of CFB attenuates renal tubulointerstitial damage by inhibiting ceramide synthesis in diabetic kidney disease. JCI Insight. ;7(24)
7. Baker ML, Kakade VR, Budiman T, Weiß M, Cunningham JM, Sadarangani S et al (2025) Spatial analysis reveals the cellular microenvironments and mechanisms of inflammation and kidney injury in acute interstitial nephritis. bioRxiv. :2025.10.29.684811
8. Reck M, Baird DP, Veizades S, Sutherland C, Bell RMB, Hur H et al (2025) Multiomic analysis of human kidney disease identifies a tractable inflammatory and pro-fibrotic tubular cell phenotype. Nat Commun 16(1):4745
9. Grunenwald A, Boudhabhay I, Revel M, Poillerat V, Voilin E, Majdi A et al (2025) The temporal gene expression landscape of rhabdomyolysis-induced acute kidney injury reveals the timing of complement activation. Commun Biol
10. West EE, Kemper C (2023) Complosome - the intracellular complement system. Nat Rev Nephrol 19(7):426–439
11. Afzali B, Singh P, Tajmul M, Kemper C (2025) Inside job: Roles of intracellular C3. J Allergy Clin Immunol
12. King BC, Kulak K, Krus U, Rosberg R, Golec E, Wozniak K et al (2019) Complement Component C3 Is Highly Expressed in Human Pancreatic Islets and Prevents beta Cell Death via ATG16L1 Interaction and Autophagy Regulation. Cell Metab 29(1):202–210 e6
13. Liszewski MK, Kolev M, Le Friec G, Leung M, Bertram PG, Fara AF et al (2013) Intracellular complement activation sustains T cell homeostasis and mediates effector differentiation. Immunity 39(6):1143–1157
14. Niyonzima N, Rahman J, Kunz N, West EE, Freiwald T, Desai JV et al (2021) Mitochondrial C5aR1 activity in macrophages controls IL-1beta production underlying sterile inflammation. Sci Immunol 6(66):eabf2489
15. Friscic J, Bottcher M, Reinwald C, Bruns H, Wirth B, Popp SJ et al (2021) The complement system drives local inflammatory tissue priming by metabolic reprogramming of synovial fibroblasts. Immunity 54(5):1002–21e10
16. Elvington M, Liszewski MK, Bertram P, Kulkarni HS, Atkinson JP (2017) A C3(H20) recycling pathway is a component of the intracellular complement system. J Clin Invest 127(3):970–981
17. Chavez LO, Leon M, Einav S, Varon J (2016) Beyond muscle destruction: a systematic review of rhabdomyolysis for clinical practice. Crit Care 20(1):135

18. Boudhabhay I, Poillerat V, Grunenwald A, Torset C, Leon J, Daugan MV et al (2021) Complement activation is a crucial driver of acute kidney injury in rhabdomyolysis. Kidney Int 99(3):581–597
19. Huang X, Zhao W, Zhang L, Yang X, Wang L, Chen Y et al (2018) The role of complement activation in rhabdomyolysis-induced acute kidney injury. PLoS ONE 13(2):e0192361
20. Boudhabhay I, Artero MR, Vasilev V, Redissi A, Peliconi J, Majdi A et al (2025) In situ Complementomics enables spatial complement activation profiling and identification of therapeutic targets across human tissues. preprint, ResearchSquare, under review
21. Petitprez F, Levy S, Sun CM, Meylan M, Linhard C, Becht E et al (2020) The murine Microenvironment Cell Population counter method to estimate abundance of tissue-infiltrating immune and stromal cell populations in murine samples using gene expression. Genome Med 12(1):86
22. Hu J, Wang SG, Hou Y, Chen Z, Liu L, Li R et al (2024) Multi-omic profiling of clear cell renal cell carcinoma identifies metabolic reprogramming associated with disease progression. Nat Genet 56(3):442–457
23. Glube N, Giessl A, Wolfrum U, Langguth P (2007) Caki-1 cells represent an in vitro model system for studying the human proximal tubule epithelium. Nephron Exp Nephrol 107(2):e47–56
24. Belliere J, Casemayou A, Ducasse L, Zakaroff-Girard A, Martins F, Iacovoni JS et al (2015) Specific macrophage subtypes influence the progression of rhabdomyolysis-induced kidney injury. J Am Soc Nephrol 26(6):1363–1377
25. Balzer MS, Doke T, Yang YW, Aldridge DL, Hu H, Mai H et al (2022) Single-cell analysis highlights differences in druggable pathways underlying adaptive or fibrotic kidney regeneration. Nat Commun 13(1):4018
26. Schubart A, Anderson K, Mainolfi N, Sellner H, Ehara T, Adams CM et al (2019) Small-molecule factor B inhibitor for the treatment of complement-mediated diseases. Proc Natl Acad Sci U S A 116(16):7926–7931
27. Clark JZ, Chen L, Chou CL, Jung HJ, Lee JW, Knepper MA (2019) Representation and relative abundance of cell-type selective markers in whole-kidney RNA-Seq data. Kidney Int 95(4):787–796
28. Li Y, Ivica NA, Dong T, Papageorgiou DP, He Y, Brown DR et al (2020) MFSD7C switches mitochondrial ATP synthesis to thermogenesis in response to heme. Nat Commun 11(1):4837
29. Kiss MG, Papac-Milicevic N, Porsch F, Tsiantoulas D, Hendrikx T, Takaoka M et al (2023) Cell-autonomous regulation of complement C3 by factor H limits macrophage efferocytosis and exacerbates atherosclerosis. Immunity 56(8):1809–24e10
30. Farrar CA, Zhou W, Lin T, Sacks SH (2006) Local extravascular pool of C3 is a determinant of postischemic acute renal failure. FASEB J 20(2):217–226
31. Farrar CA, Tran D, Li K, Wu W, Peng Q, Schwaeble W et al (2016) Collectin-11 detects stress-induced L-fucose pattern to trigger renal epithelial injury. J Clin Invest 126(5):1911–1925
32. Pratt JR, Basheer SA, Sacks SH (2002) Local synthesis of complement component C3 regulates acute renal transplant rejection. Nat Med 8(6):582–587

33. Laskowski J, Philbrook HT, Parikh CR, Thurman JM (2019) Urine complement activation fragments are increased in patients with kidney injury after cardiac surgery. Am J Physiol Ren Physiol 317(3):F650–F7
34. Huang E, Vo A, Choi J, Ammerman N, Lim K, Sethi S et al (2020) Three-Year Outcomes of a Randomized, Double-Blind, Placebo-Controlled Study Assessing Safety and Efficacy of C1 Esterase Inhibitor for Prevention of Delayed Graft Function in Deceased Donor Kidney Transplant Recipients. Clin J Am Soc Nephrol 15(1):109–116
35. Schroppel B, Akalin E, Baweja M, Bloom RD, Florman S, Goldstein M et al (2020) Peritransplant eculizumab does not prevent delayed graft function in deceased donor kidney transplant recipients: Results of two randomized controlled pilot trials. Am J Transpl 20(2):564–572
36. Bongoni AK, Kiss B, McRae JL, Salvaris EJ, Fisicaro N, Muntz F et al (2025) Targeting the complement lectin pathway with a highly specific MASP-2 inhibitor protects against renal ischemia-reperfusion injury. Proc Natl Acad Sci U S A 122(16):e2424754122
37. Isnard P, Laemmel E, Martinez T, Bergis B, Harrois A, Huertas A et al (2025) The Spatially Resolved Kidney Transcriptome Signatures in Rat Models of Trauma-Induced Acute Kidney Injury. Kidney360
38. Kirita Y, Wu H, Uchimura K, Wilson PC, Humphreys BD (2020) Cell profiling of mouse acute kidney injury reveals conserved cellular responses to injury. Proc Natl Acad Sci U S A 117(27):15874–15883
39. Muto Y, Dixon EE, Yoshimura Y, Ledru N, Kirita Y, Wu H et al (2024) Epigenetic reprogramming driving successful and failed repair in acute kidney injury. Sci Adv 10(32):eado2849
40. Polonsky M, Gerhardt LMS, Yun J, Koppitch K, Colon KL, Amrhein H et al (2024) Spatial transcriptomics defines injury specific microenvironments and cellular interactions in kidney regeneration and disease. Nat Commun 15(1):7010
41. Melchinger I, Guo K, Li X, Guo J, Cantley LG, Xu L (2024) VCAM-1 mediates proximal tubule-immune cell cross talk in failed tubule recovery during AKI-to-CKD transition. Am J Physiol Ren Physiol 327(4):F610–F22
42. Gerhardt LMS, Liu J, Koppitch K, Cippa PE, McMahon AP (2021) Single-nuclear transcriptomics reveals diversity of proximal tubule cell states in a dynamic response to acute kidney injury. Proc Natl Acad Sci U S A 118:27
43. Tang Z, Lu B, Hatch E, Sacks SH, Sheerin NS (2009) C3a mediates epithelial-to-mesenchymal transition in proteinuric nephropathy. J Am Soc Nephrol 20(3):593–603
44. Cho MS, Rupaimoole R, Choi HJ, Noh K, Chen J, Hu Q et al (2016) Complement Component 3 Is Regulated by TWIST1 and Mediates Epithelial-Mesenchymal Transition. J Immunol 196(3):1412–1418
45. Shimazaki R, Takano S, Satoh M, Takada M, Miyahara Y, Sasaki K et al (2021) Complement factor B regulates cellular senescence and is associated with poor prognosis in pancreatic cancer. Cell Oncol (Dordr) 44(4):937–950

46. Grunenwald A, Roumenina LT, Frimat M (2021) Heme Oxygenase 1: A Defensive Mediator in Kidney Diseases. Int J Mol Sci. ;22(4)
47. Yan B, Freiwald T, Chauss D, Wang L, West E, Mirabelli C et al (2021) SARS-CoV-2 drives JAK1/2-dependent local complement hyperactivation. Sci Immunol. ;6(58)
48. Sahu SK, Ozanturk AN, Kulkarni DH, Ma L, Barve RA, Dannull L et al (2023) Lung epithelial cell-derived C3 protects against pneumonia-induced lung injury. Sci Immunol 8(80):eabp9547
49. Kuska K, Bettoni S, Mohlin F, Chrobak M, Dandavate V, Moradi S et al (2025) Intracellular C3 regulates the immune response to infection via NF-kappaB signaling. Cell Mol Life Sci 83(1):1
50. Zhang M, Liu Q, Meng H, Duan H, Liu X, Wu J et al (2024) Ischemia-reperfusion injury: molecular mechanisms and therapeutic targets. Signal Transduct Target Ther 9(1):12

# Figures

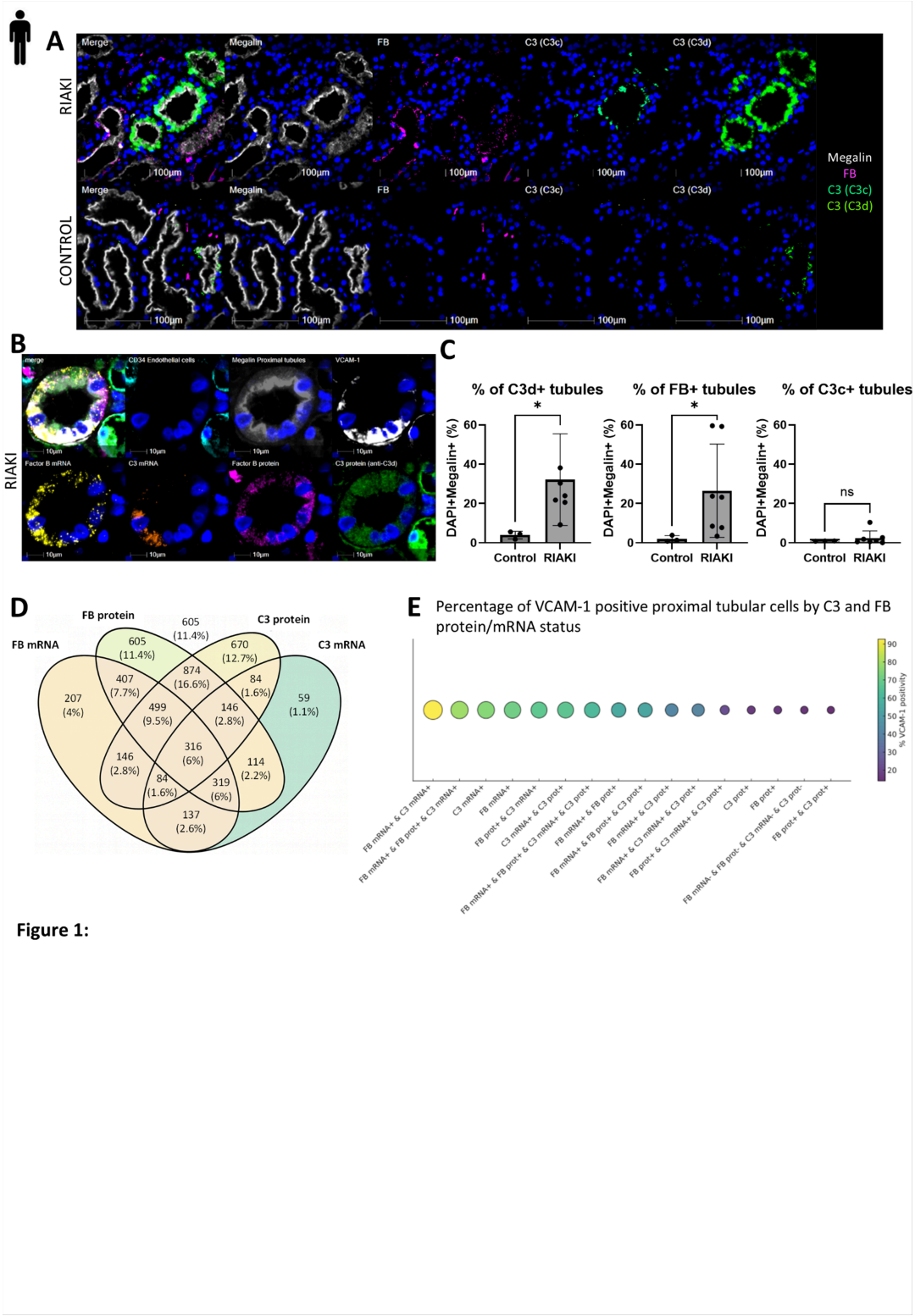



**Figure 1:**

## Figure 1

**Intracellular C3 and FB protein and mRNA are detected in injured proximal tubular cells from RIAKI patients**. (A) Detection of intracellular, granular pattern of C3 with an anti-C3d but less/no with anti-C3c recognizing antibody as well as FB in proximal tubular cells (detected by Megalin) of a RIAKI patient (top), contrary to the weak staining in control kidney biopsy (bottom) by multiplexed sequential immunofluorescence (SeqIF). Panels show merged image (left) and individual markers (megalin : white,

FB protein : pink, C3 protein detected by anti C3d or anti C3c antibody : green) (B) Multiplexed sequential immunofluorescence (SeqIF) combined with RNA scope in a RIAKI patient. Panel shows merged image (top, left) and individual markers (CD34: cyan, megalin: grey, VCAM-1: white, FB mRNA: yellow, C3 mRNA: orange, FB protein: pink, C3 protein detected by anti C3d antibody: green). Detection of colocalization of protein and mRNA staining for C3 and FB in a fraction of the activated (VCAM-1+) proximal tubular cells (Megalin+). In another portion of the proximal tubules, protein but not mRNA were detected. C) % of proximal tubules, positive for staining with anti-C3d, anti-FB and anti-C3c antibody in RIAKI vs control kidney biopsies, quantification by Halo software. (D) Venn diagram for the number of tubular cells positive for C3 protein and/or mRNA and FB protein and/or mRNA in the tested patient biopsy. E) Percentage of VCAM-1 positive proximal tubular cells by C3 and FB protein/mRNA status. * $p<0.05$, Mann Whitney test for pairwise comparison.

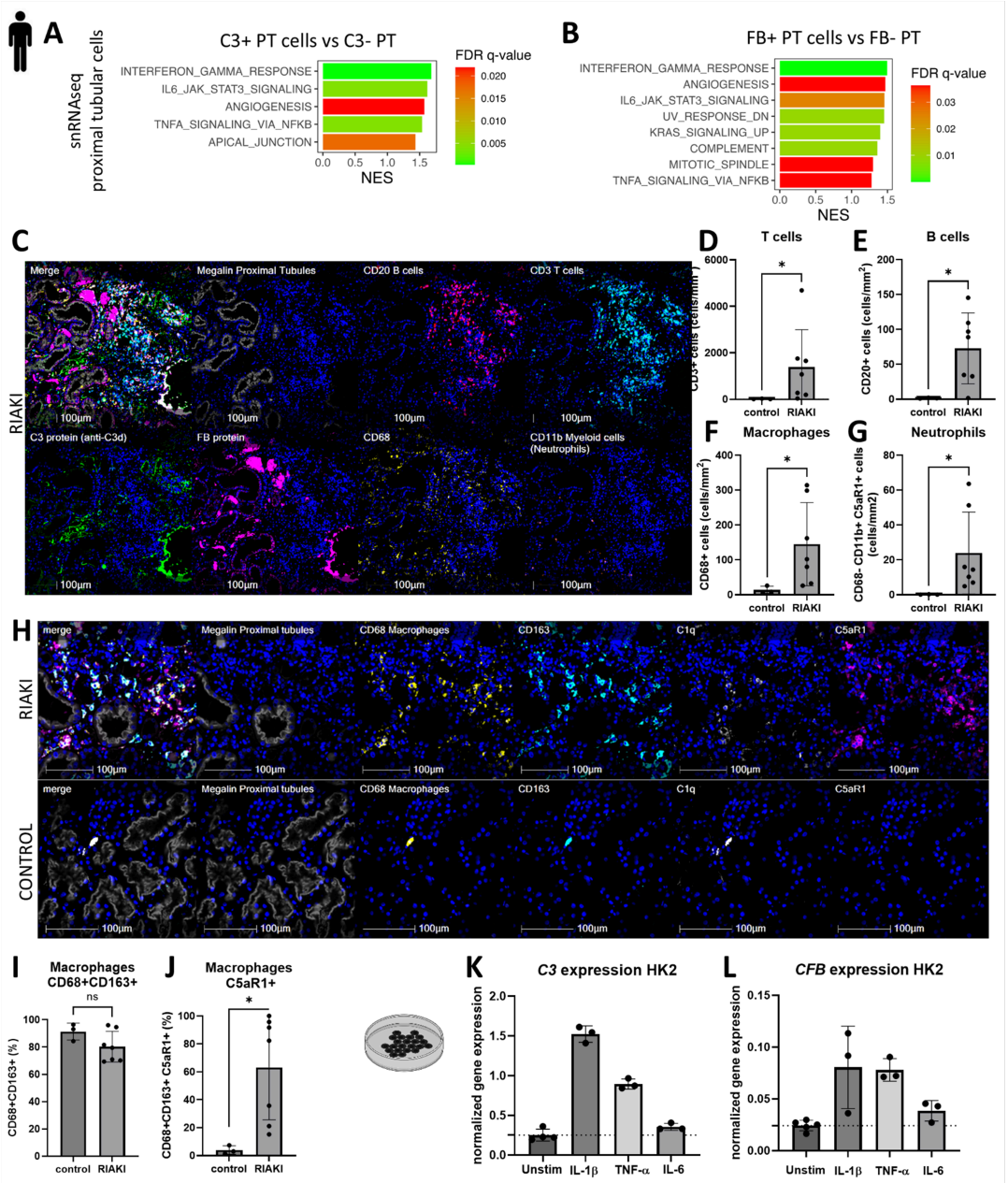



Figure 2.

## Figure 2

**C3 and FB are expressed in patients and *in vitro* by proximal tubular cells under inflammatory stimulation.** (A-B) GSEA of A) C3 and B) CFB expressing human proximal tubular cells in normal kidney tissue (peritumoral) derived from a single nuclei (sn) RNAseq dataset from Hu et al., 2024. (C-J) Inflammatory immune infiltrates in kidney biopsies from RIAKI patients detected by SeqIF. (C) Representative SeqIF image of immune infiltrates in RIAKI biopsies by multiplexed sequential

immunofluorescence (SeqIF) . Panels show merged image (top left) and individual markers: proximal tubules (Megalin, grey), B cells (CD20, red), T cells (CD3, cyan), macrophages (CD68, yellow), myeloid cells including neutrophils (CD11b, orange), C3 protein (anti-C3d, green), and factor B protein (FB, pink). Nuclei are counterstained with DAPI (blue). Scale bars, 100 μm. (D-G) Quantification of immune infiltrates in 7 RIAKI patients compared with 3 normal kidney biopsies for T cells ($CD3^+$; D), B cells ($CD20^+$; E), macrophages ($CD68^+$; F), and neutrophils ($CD68^-CD11b^+$; G). (H) Phenotype of macrophages infiltrating RIAKI kidneys compared with normal kidney biopsies. Panels show proximal tubules (Megalin, grey), macrophages (CD68, yellow), and phenotype markers CD163 (cyan), C1q (white), and C5aR1 (magenta). (I) Proportion of macrophages ($CD68^+$) positive for CD163 in control and RIAKI kidneys. (J) Proportion of $CD68^+CD163^+$ macrophages positive for C5aR1 in control and RIAKI kidney biopsies. (K) *C3* and (L) *CFB* gene expression is stimulated by AKI-relevant inflammatory mediators in proximal tubular cell line HK2. Gene expression detected by QuantiGene. Unstim – unstimulated cells. * $p<0.05$, Mann Whitney test for pairwise comparison.

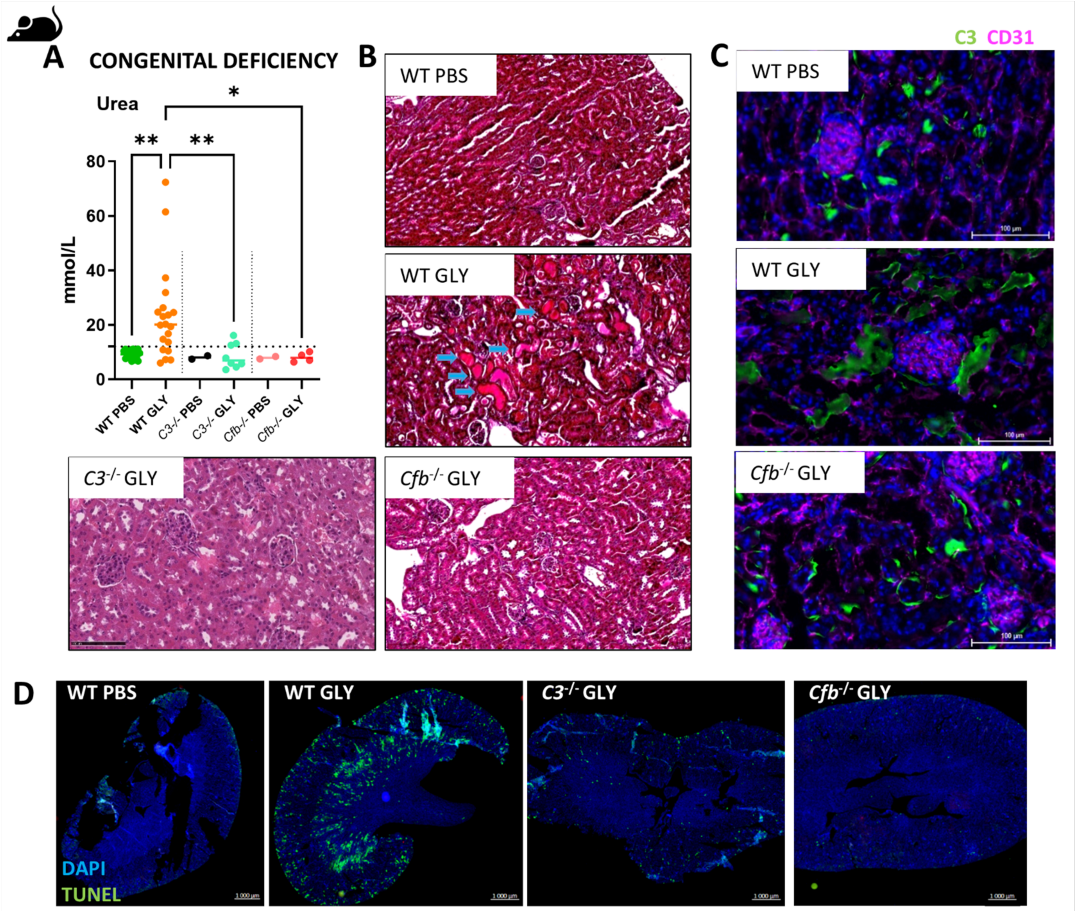



Figure 3

## Figure 3

**Mice deficient for C3 or FB are protected from AKI in a rhabdomyolysis model** (A) Kidney injury (renal function) measured by blood urea nitrogen (BUN) in WT PBS-injected mice (green), WT-glycerol (GLY) mice (orange) and deficient for *C3*$^{-/-}$ PBS (blue) or GLY (turquoise) mice, or *Cfb*$^{-/-}$ PBS (pink) or GLY (red) mice. The horizontal dotted line indicates the normal range, determined by the average + 2SD of the value measured for the PBS treated group. The presented results are from total of 21 PBS and 21 GLY

injected WT mice; 2 PBS and 4 GLY injected *Cfb*$^{-/-}$ mice; and 2 PBS and 8 GLY *C3*$^{-/-}$ mice. (B) Hematoxylin/eosin staining on paraffin-embedded kidneys 24 hours after injection by PBS (WT PBS) or glycerol (WT GLY) or after glycerol injection in *Cfb*$^{-/-}$ (*Cfb*$^{-/-}$ GLY) or *C3*$^{-/-}$ (*C3*$^{-/-}$ GLY) mice. Original magnification 20x. Blue arrows indicate myoglobin casts. (C) Double staining of C3b (green) and CD31 (magenta) immunofluorescence on WT-PBS, WT-GLY, FB-/- GLY mice. (D) TUNEL staining on kidney of WT-PBS (left), WT-GLY (middle left), *C3*$^{-/-}$ (middle right) and *Cfb*$^{-/-}$ (right) mice, original magnification 20x.

* p<0.05, ** p<0.01, *** p<0.001, **** p < 0.0001, Kruskal Wallis test with Benjamini, Krieger and Yekutieli correction for multiple comparisons.

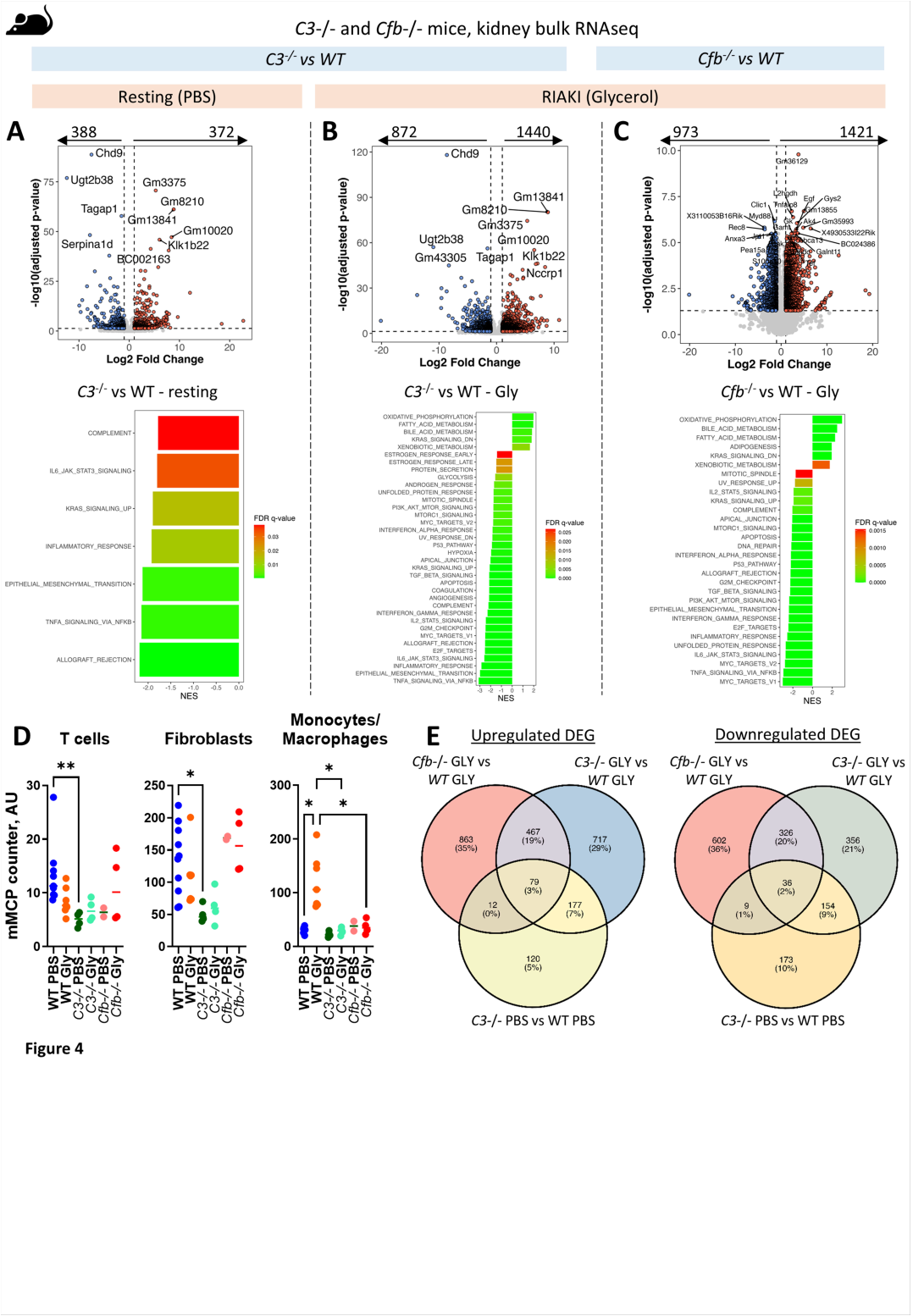



Figure 4

## Figure 4

**C3 and FB deficiency in mice induce potent transcriptomic reprogramming of the kidney in the RIAKI model.** (A) Volcano plot of gene expression in *C3*$^{-/-}$ versus WT mice at resting state (PBS condition) (top). GSEA of the hallmark gene-sets that are significantly different in *C3*$^{-/-}$ PBS mice as compared to WT PBS (bottom). (B) Volcano plot of gene expression in Gly-treated *C3-/-* versus WT mice' kidneys (top). GSEA of the hallmark gene-sets that are significantly different in *C3*$^{-/-}$ mice as compared to WT 24 hours after

Gly injection (bottom). (C) Volcano plot (top) and GSEA of the hallmark gene-sets of the *Cfb*-/- mice, analyzed as the *C3*$^{-/-}$ ones (bottom). (D) Estimating the population abundance of kidney-infiltrating T cells, fibroblasts and inflammatory monocytes by the mMCP-counter tool in the *C3* and *Cfb*$^{-/-}$ mice compared to WT in the RIAKI model. (E) Venn diagrams of the common up or down-regulated DEG (genes with an absolute log fold change >1 and an adjusted p-value of less than 0,05 are differentially expressed (DEG) between the control and the test groups) between the *C3*-/- PBS vs WT PBS , *C3*$^{-/-}$ GLY vs *WT* GLY and *Cfb*$^{-/-}$ GLY vs *WT GLY* mouse kidneys. (A, B, C bottom) Shown are the gene-sets with FDR threshold FDR<0.25 and FDR q-value p<0.05. Plotted is the Normalised Enrichment Score (NES). * p<0.05 Kruskal Wallis test with Benjamini, Krieger and Yekutieli correction for multiple comparisons.

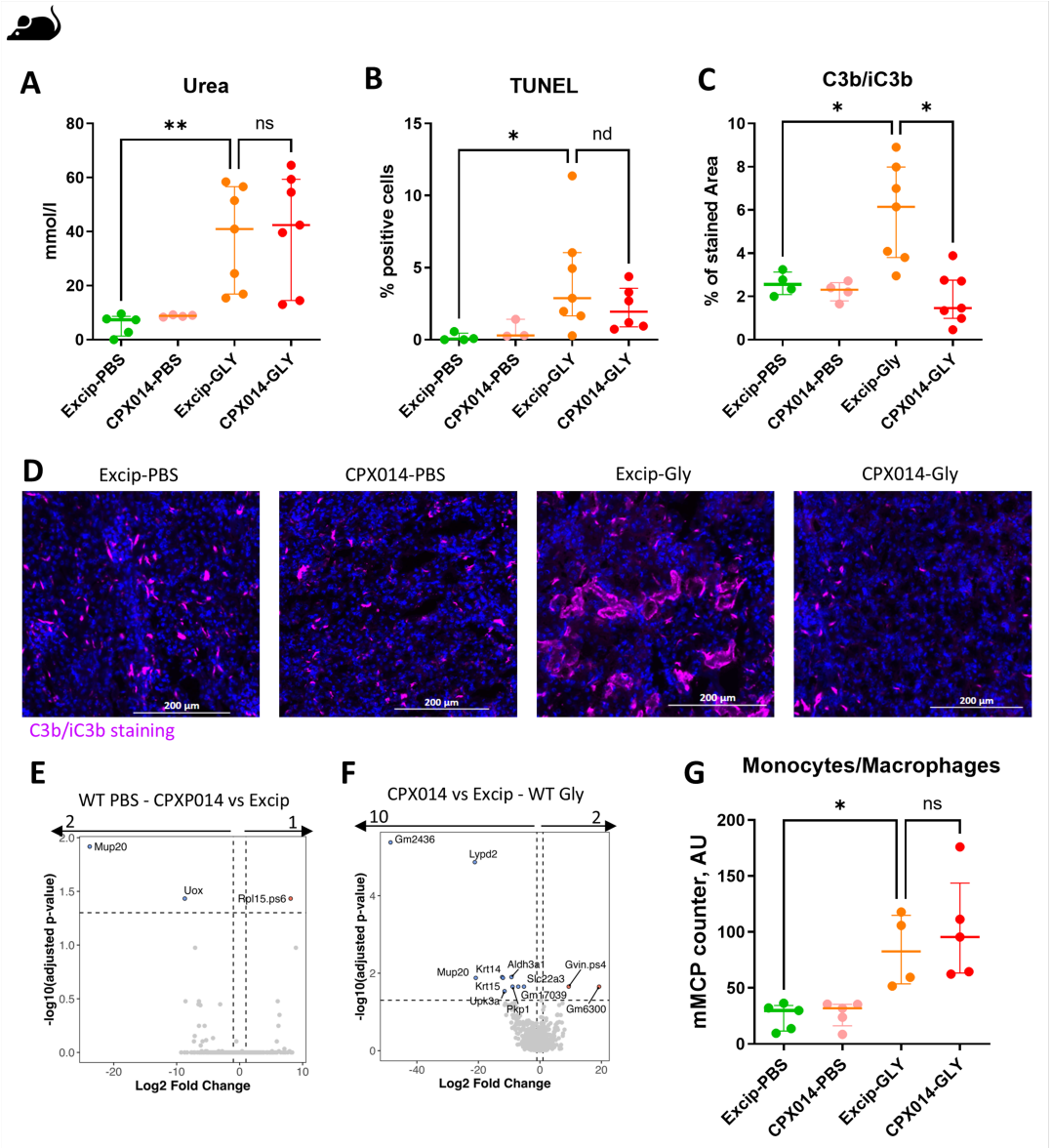



**Figure 5**

## Figure 5

**Inhibition of complement cascade does not protect the WT mice in the rhabdomyolysis model.**

A) Kidney injury (renal function) measured by blood urea nitrogen (BUN) in WT mice injected by PBS or glycerol (GLY), in mice preventively treated by FB inhibitor CPX014 as compared to excipient (Excip). The presented results are from one experiment with 5 Excip/PBS, 4 CPX014/PBS, 7 Excip/GLY, 7

CPX014/GLY injected mice. B) Quantification of the TUNEL staining for apoptosis. C) Quantification of the C3 staining in the kidney. Quantification of the % area of C3b deposits on snap-frozen kidney by immunofluorescence, evaluated by HALO software upon FB inhibition. D) Examples of C3b/iC3b staining (magenta) of mouse kidney. Nuclear staining (Dapi) is in blue. (E-G) Transcriptomic analysis of the kidneys of the glycerol-injected mice, pre-treated with FB inhibitor CPX014 or excipient (Excip). Volcanoplots of E) control or F) Gly-injected mice. G) Estimating the population abundance of kidney-infiltrating inflammatory monocytes by mMCP-counter tool. * $p<0.05$, ** $p<0.01$, *** $p<0.001$, **** $p < 0.0001$, Kruskal Wallis test with Benjamini, Krieger and Yekutieli correction for multiple comparisons.

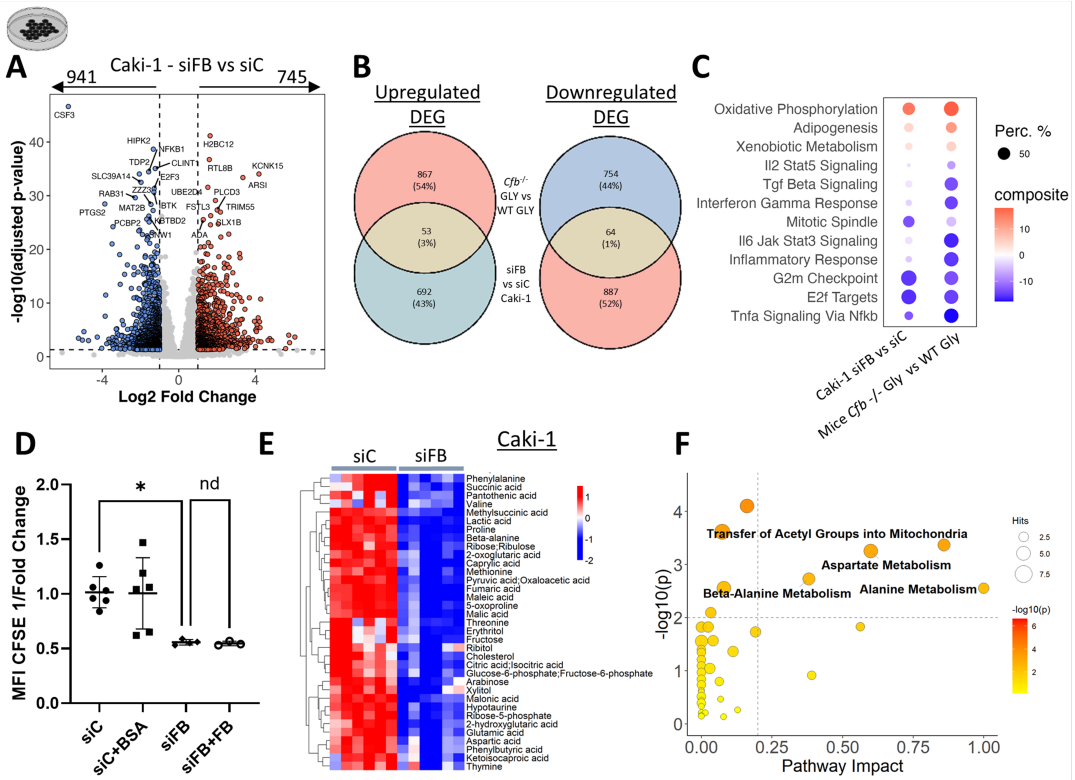



**Figure 6**

## Figure 6

**FB knockdown in a proximal tubular cell *in vitro* model recapitulates the phenotype of the mouse kidney through a cell-intrinsic mode of action**. A) Volcano Plot representing differentially expressed genes (absolute log2 fold change >1 and an adjusted p-value < 0,05) upon FB knockdown in Caki-1 cells evaluated by RNA sequencing. B) Venn diagram showing the common un and down-regulated DEG between the *Cfb*-/- mice and siFB cells. C) Comparison of the Hallmark gene sets among the siFB Caki1

cells and the Gly-injected *Cfb-/-* mice. D) Proliferation test (CFSE signal dilution) for siC and siFB Caki-1 cells in presence or absence of purified FB or BSA as a control. E) Heatmap of the significantly up or downregulated metabolites in siFB cells (blue-up; red-down), detected by mass spectrometry. F) Significantly impacted metabolic pathways. * p<0.05, ** p<0.01, Kruskal Wallis test with Benjamini, Krieger and Yekutieli correction for multiple pairwise comparison.

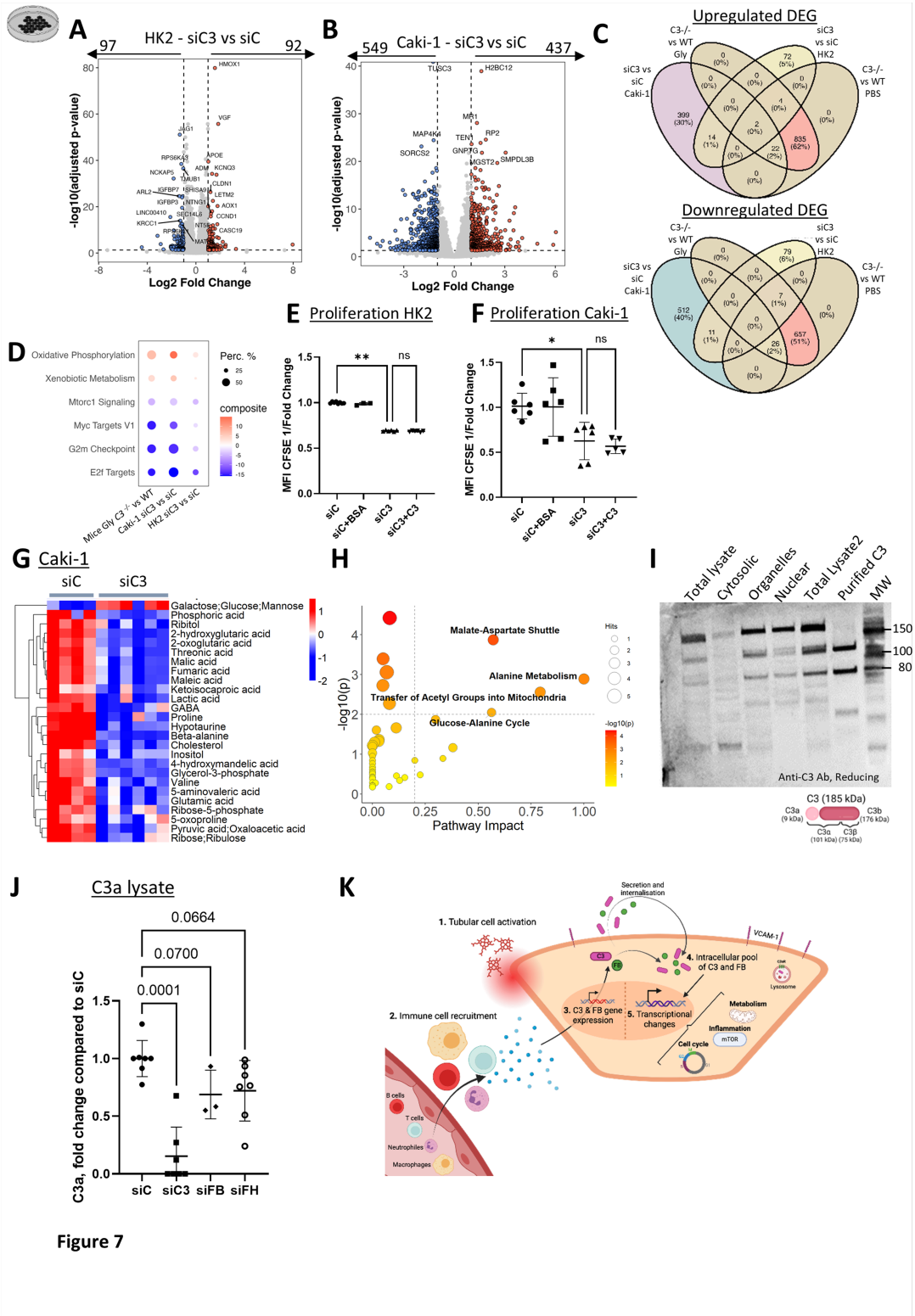



**Figure 7**

**C3 knockdown in proximal tubular cell *in vitro* models partially recapitulates the phenotype of the C3-/- mouse kidney through a cell-intrinsic mode of action**. (A-B) Volcano Plot representing differentially expressed genes (absolute log2 fold change >1 and an adjusted p-value < 0,05) upon C3 knockdown in A) HK2 cells and B) Caki-1 evaluated by RNA sequencing. C) Venn diagram comparing the up and down-regulated DEG between the two in vitro and the two in vivo models of C3 deficiency. D) Common Hallmark gene sets between Gly-treated C3-deficient mice, siC3 HK2 and Caki-1 cells. (E-F) Proliferation test (CFSE signal dilution) for siC and siC3 E) HK2 cells and F) Caki-1 in presence or absence of purified C3 or BSA as a control. G) Targeted metabolomic analysis of the lysate of Caki-1 cells. Heatmap of the significantly up or downregulated metabolites in siC3 cells (blue-up; red-down). H) Significantly impacted metabolic pathways. I-J) Exploration whether FB modulates cell functions by cleaving intracellular C3 or not. I) Detection of C3 in the total lysate and sub-cellular fractions of Caki-1 by western blot with anti-C3 polyclonal Ab, reducing conditions. The ~170 kDa band corresponds to an unprocessed form of C3, the 110 kDa band to the a-chain of C3 and the 75 kDa band – to the b-chain of processed C3. Schema of the chains and fragments of C3. J) Evaluation of the process of C3a generation by silencing its source protein C3, the potential cleaving enzyme FB and the potential regulator FH. C3a levels in the lysate of Caki-1 cells, silenced for C3, FB or FH measured by ELISA. K) Proliferation test (CFSE signal dilution) for siC3aR compared to siC and siC3. * p<0.05, ** p<0.01, *** p<0.001, **** p < 0.0001, Kruskal Wallis test with Benjamini, Krieger and Yekutieli correction for multiple comparisons. L) Schematic representation of the proposed hypothesis of a cross-talk between myoglobin/heme injured proximal tubules in the context of RIAKI with the immune infiltrate in the kidney, leading to C3 and FB overexpression and reabsorption from the extracellular space. The cell-intrinsic C3 and FB promote by different modes of action an inflammatory and proliferative phenotype, metabolism reprogramming and increased susceptibility to AKI.

## Supplementary Files

This is a list of supplementary files associated with this preprint. Click to download.

- Grunenwaldetalsupplementaryfigures.pdf
- GrunenwaldetalSupplementaryMethodsfinal.pdf
- UncutWB.pdf
- SupplementaryDataCommonupanddownregulatedDEG.xlsx